Draft version December 5, 2024
Typeset using LaTeX **twocolumn** style in AASTeX631

How Many Bursts Does it Take to Form a Core at the Center of a Galaxy?

Olivia Mostow [1], Paul Torrey [1], Jonah Rose [2], Alex M. Garcia [1], Niusha Ahvazi [1], Mariangela Lisanti [3,4] and Nitya Kallivayalil [1]

[1] *Department of Astronomy, University of Virginia, 530 McCormick Road, Charlottesville, VA 22903, USA*
[2] *Department of Astronomy, University of Florida, Gainesville, FL 32611, USA*
[3] *Center for Computational Astrophysics, Flatiron Institute, 162 5th Avenue, New York, NY 10010, USA*
[4] *Department of Physics, Princeton University, Princeton, NJ 08544, USA*

ABSTRACT

We present a novel method for systematically assessing the impact of central potential fluctuations associated with bursty outflows on the structure of dark matter halos for dwarf and ultra-faint galaxies. Specifically, we use dark-matter-only simulations augmented with a manually-added massive particle that modifies the central potential and approximately accounts for a centrally-concentrated baryon component. This approach enables precise control over the magnitude, frequency, and timing of when rapid outflow events occur. We demonstrate that this method can reproduce the established result of core formation for systems that undergo multiple episodes of bursty outflows. In contrast, we also find that equivalent models that undergo only a single (or small number of) burst episodes do not form cores with the same efficacy. This is important because many ultra-faint dwarf (UFD) galaxies in the local universe are observed to have tightly constrained star formation histories that are best described by a single, early burst of star formation. Using a suite of cosmological, zoom-in simulations, we identify the regimes in which single bursts can and cannot form a cored density profile, and therefore, can or cannot resolve the core-cusp problem.

Keywords: Galaxy dark matter halos(1880) — Galaxy structure(622) — Cold dark matter(265)

1. INTRODUCTION

The current paradigm of cold, collisionless dark matter plus dark energy (ΛCDM) has had a number of successes reproducing observations on the largest scales. For example, the distribution of galaxy clusters seen from large sky surveys are consistent with the predictions of cosmological N-body simulations which evolve the primordial fluctuations measured from the CMB to present-day using a ΛCDM framework (e.g., Springel et al. 2005; Reid et al. 2010). Yet, on smaller scales (i.e., the scales of individual galaxies), key tensions persist that bring into question whether a cold and collisionless dark matter species is indeed the best descriptor of dark matter (Bullock & Boylan-Kolchin 2017; Sales et al. 2022).

The small scale tensions in ΛCDM generally arise from inconsistencies in the structure, abundance, or distribution of galaxies as predicted from ΛCDM when compared against observations—especially for low mass systems (Moore 1994; Sales et al. 2022). Among them, the "core-cusp" problem identifies a tension whereby ΛCDM galactic halos are expected to follow NFW profiles (Navarro et al. 1996b) which feature a continuously rising central dark matter density (i.e. a dark matter cusp) with an inner log-slope $\frac{dlog(\rho)}{dlog(\mathrm{r})}$ that approaches -1 at small radii, whereas it is observationally inferred that some nearby low-mass galaxies have a flattened inner dark matter density (i.e. a dark matter core). Such an inconsistency may be an indication that the Cold Dark Matter (CDM) model that underpins our current cosmological paradigm needs revisiting.

Indeed, alternative dark matter models—which generally encompass (i) modified initial matter power spectra, (ii) modified self-interactions, or (iii) dark matter equations of motion governed by more than gravity alone—can potentially solve many of the small scale tensions (see e.g., Sales et al. 2022). For example, the inclusion of dark matter self-interactions (e.g., Spergel & Steinhardt 2000; Tulin & Yu 2018) has been shown to flatten the inner DM density by increasing the efficiency of heat transfer in the interior regions (Vogelsberger et al. 2014; Burger et al. 2022; Jahn et al. 2023; Shen et al. 2024).

Yet it is worth noting that this tension was initially identified and studied through N-body simulations which lack a direct treatment of the baryonic component of galaxies. Modern cosmological simulations include not only gravity acting upon dark matter, but also hydrodynamics coupled to comprehensive models of galaxy formation. These simulations incorporate the physics of gas cooling, stellar feedback, AGN feedback, star formation, black holes, and the ISM (see, e.g., Somerville & Davé 2015; Vogelsberger et al. 2020, for reviews). The inclusion of baryons is not just an improvement allowing for more direct modeling of the emergent galaxy population, but is also critical for the evaluation of the ΛCDM tensions as the baryons can impact the dark matter by modifying the overall halo potential.

In fact, it has been demonstrated that the interaction of dark matter and baryons through gravity alone may be sufficient to alleviate the core-cusp problem (Navarro et al. 1996a; Read & Gilmore 2005; Governato et al. 2012). Episodic mass ejection from the galactic center can inject heat into the central DM by rapidly fluctuating the central potential (Governato et al. 2010; Pontzen & Governato 2012, 2014). Physically, these episodic mass ejections can be thought of as strong, or "bursty", stellar feedback events. Fully cosmological simulations employing the more bursty feedback models have shown core formation beginning in the classical dwarf ($M_* = 10^5$–10^7 $M_\odot$) regime and peaking in strength for bright dwarf ($M_* = 10^7$–10^9 $M_\odot$) galaxies (Chan et al. 2015; Tollet et al. 2016; Bullock & Boylan-Kolchin 2017; Lazar et al. 2020; Di Cintio et al. 2014; Azartash-Namin et al. 2024). Thus, if star formation occurs in stochastic bursts (e.g. Governato et al. 2010; Hayward & Hopkins 2017; Faucher-Giguère 2018), as opposed to the stellar mass growing smoothly over time, the resulting gaseous outflows naturally perturb the orbits of the DM particles in the inner region and sufficiently flatten the density profile (e.g. Oñorbe et al. 2015; Jahn et al. 2023). There are, however, limits where stellar feedback is incapable of dark matter core formation. Fitts et al. (2017) found $M_* \approx 2 \times 10^6$ $M_\odot$ to be the threshold mass for bursty feedback to significantly modify the DM density profile. This limit is primarily, if not entirely, an energetic one: galaxies that are too low in mass simply do not have enough stellar feedback energy present to convert the core into a cusp.

Regardless of the details, it is clear that the small-scale tensions may arise either owing to our lack of knowledge of galaxy formation physics or a fundamental flaw in our currently favored dark matter paradigm. Studying both (i) the regimes when, where, and how bursty feedback is able to operate and, separately, (ii) the regimes where bursty feedback is able to convert dark matter cusps into cores is therefore critical to our understanding of the extent to which our dark matter prescription needs to be modified. In this work, we take a new approach of using fully cosmological, dark-matter-only (DMO) simulations coupled to analytically-modulated central potential contributions. We are able to capture the fully cosmological development of the dark matter halo, while also considering how *systematically varied* time-dependent central potentials impact the dark matter halo structure. Moreover, as we demonstrate within this paper, we can systematically vary the total number of bursts, as well as the total mass ejected in each burst. Our approach allows us to fill in an important void that sits between previous idealized studies (e.g., those of Pontzen & Governato 2012) and the fully cosmological studies where the bursty nature of feedback naturally arises in a way that cannot be directly modulated (e.g., Hopkins et al. (2014); Oñorbe et al. (2015); Lazar et al. (2020); Chan et al. (2015)).

In addition to introducing this flexible framework, we also aim to address the questions: "Could galaxies convert a dark matter cusp into a core via a single episode of star formation?" It has been suggested that some ultra-faint dwarf satellite galaxies have implied cored dark matter density profiles (Almeida et al. 2024). However, the stellar populations within these systems are fairly tightly constrained to be consistent with approximately single age stellar populations that are also very old (i.e. having formed $> 80\%$ of their stellar mass before the midpoint of reionization ($z = 7.7 \pm 0.7$; Sacchi et al. 2021). In other words, if these systems formed most of their stellar mass in a single burst long ago, could that be sufficient to convert dark matter cusp into a core, or are multiple, episodic bursts required?

In this paper, we test the ability of bursty feedback to convert cusps into cores using modified cosmological simulations where we can manually prescribe the number and magnitude of the bursts to address this question. The structure of this paper is as a follows. In §2, we outline our methods including a description of our simulations (§2.1), the employed galaxy growth/burst/outflow models (§2.2, §2.3) and method of characterizing inner dark matter density profiles (§2.4). In §3, we present our results, split into the classical dwarf (§3.1) and ultrafaint dwarf (§3.2) regimes. In §4, we discuss our results and in §5, we present our conclusions.

2. METHODS

2.1. *Simulations*

We study the mechanism of core formation via bursty feedback using modified cosmological simulations. The

foundation of our cosmological simulations are standard DMO zoom-in simulations. We create zoom-in initial conditions using MUSIC (Hahn & Abel 2011), with a parent box of 36 Mpc. We adopt cosmological parameters $\Omega_0 = 0.301712$, $\Omega_\Lambda = 0.6983$, $\Omega_b = 0.0$, and $H_0 = 100$ h km s^{-1} where $h = 0.6909$ consistent with Planck Collaboration XI (Planck Collaboration et al. 2016). Our simulations have a dark matter mass resolution of $3.44 \times 10^3 M_\odot$ and a gravitational softening of 0.038 kpc. We then evolve these initial conditions from redshift $z = 127$ down to $z = 0$ using the simulation code AREPO (Springel 2010; Weinberger et al. 2020). Prior to the addition of any changes to the central potential (as described below), the setup described here is a standard CDM cosmological zoom-in simulation.

Our goal in this paper is to probe the impact of a set of successive mass expulsion events on the resulting dark matter halo structure. To achieve this, we follow the approach used in Rose et al. (2023) whereby the gravitational impact of the central baryon component (i.e. galactic gas and stars) is represented by a single massive simulation particle. Unlike the dark matter simulation particles, which move freely under the force of gravity through the simulation domain and have a constant mass with time, the tracer particle is pinned to the potential minimum of the halo and given a manually-prescribed mass that evolves with time. As with all other simulation particles, the tracer particle is assigned a gravitational softening. While this is strictly to avoid two-body interactions for dark matter particles, a larger softening is employed for the massive tracer particle to emulate the effect of having a spatially-distributed (i.e. not point-like) mass distribution. We note that a different potential modification profile could have been selected, however, Rose et al. (2023) showed this was sufficient to produce realistic galaxy properties when compared with baryonic simulations.

We note three points about this setup. First, because we manually vary the tracer particle's mass, the total mass in the simulation is not conserved. This variation in the particle's mass can capture the impact of baryons condensing into the central region and subsequently being expelled. In other words, this particle is the mechanism that we use to impose specific time variability in the central potential. We do not expect the fact that the global mass budget changes slightly with time to impact our findings. While local fluctuations to the mass (i.e. bursty outflows) can change the distribution of matter in the central halo, these fluctuations amount to a change in the total mass globally that is of order 10^{-6}%. Second, even though we are using a very simplistic method for modifying the central potential, the approach does capture the impact of the central baryon component on the dark matter halo structure, as demonstrated in Rose et al. (2023). And, third, because we are manually prescribing the tracer particle's mass, we can systematically explore varied mass growth histories including an array of smooth and bursty growth histories.

We first explore the classical dwarf regime in order to ensure the model can reproduce previous results for the central dark matter halo properties in the presence and absence of bursty feedback. We first model the smoothly forming classical dwarf galaxy (i.e. without bursty feedback) to verify cusp formation. We then model the same system with the stellar mass forming over multiple episodic bursts of star formation. Finally, we compare the resulting dark matter density profiles to verify that the tracer particle emulating bursty outflows can turn the cusp to a core. Once this is established, we apply this method to the specific case of ultra-faint dwarfs that undergo just one outflow.

2.2. *Galaxy Growth/Outflow Models*

The unique feature of our simulations is that we impose specific mass evolution histories on the tracer particle. Specifically, its mass is updated at each timestep during the simulation following some pre-prescribed pattern. We employ three growth patterns: a smooth growth model, an episodically bursty model, and a single burst model—each of which are described here.

The first class of model is a smooth star formation history, henceforth referred to as smooth growth models, which describes a galaxy whose central mass smoothly grows with time (i.e. does not experience any significant mass blowouts). The tracer mass growth over time for this model is shown in the top right panel of Figure 1. The primary purpose of these models is to provide a standard of comparison against which we can understand how the bursts have (or have not) impacted the density profile.

The second class of model is the episodically bursty model, where the galaxy is assumed to accrete gas mass smoothly for some period of time, followed by a rapid/instantaneous drop in the tracer particle mass mimicking a feedback-driven blowout event. The tracer mass growth over time for one such model is shown in the lower right panel of Figure 1. We keep the final stellar mass fixed at the same value as in the smooth model (described in further detail for each of the two galaxy models in 2.3). We prescribe a mass evolution for the tracer particle that is meant to mimic the fluctuating mass of a galaxy with bursty outflows and captures the impact that bursty feedback has on the orbits of

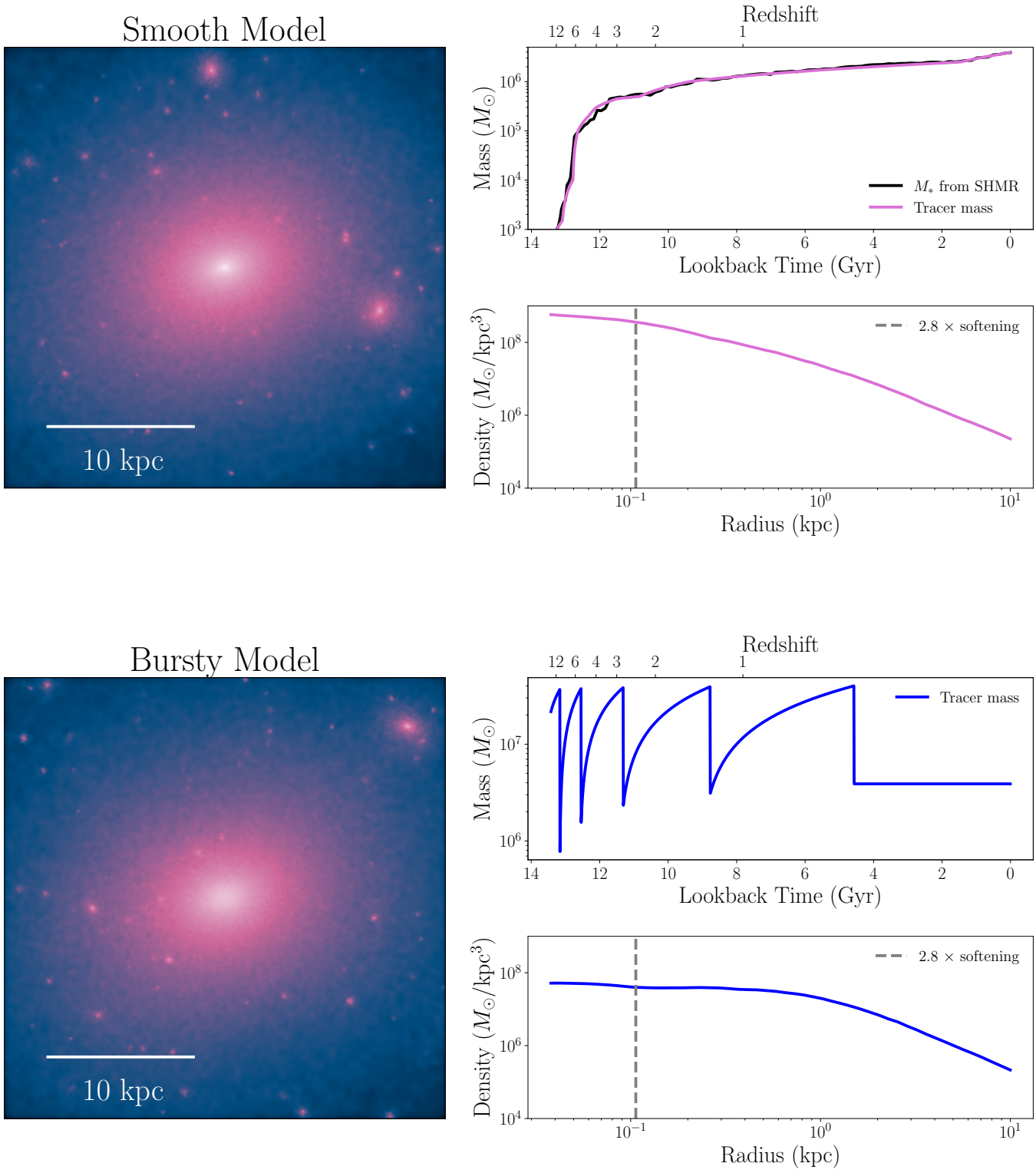

Figure 1. Comparison of dark matter density for the smooth (top panels) and bursty (bottom panels) models implemented using the modified-DMO approach for a halo with mass $9.2 \times 10^9 M_\odot$. *Left:* Dark matter mass projection made from a $30 \times 30 \times 30$ kpc box surrounding the central halo. The halos look similar, save for their central regions. The smooth growth model produces a clear peak in density at the very center, while the bursty model reaches a constant density (forms a core) up to ~ 2.0 kpc from the center. *Right:* Tracer mass versus time as well as density profile for the smooth growth and bursty model. In both cases, the final stellar mass is $3.9 \times 10^6 M_\odot$. The tracer mass in the upper panel represents a galaxy with a smooth growth history, which follows the SHMR shown in black. The tracer mass evolution in the lower panel represents a galaxy that undergoes 5 bursts of star formation, expelling $3.6 \times 10^7 M_\odot$ of gas in each burst. The $z = 0$ dark matter density profiles produced from each of these models are also shown. The grey dashed line marks $2.8\times$ the dark matter particle softening, the point below which numerical effects begin to be important. The smooth growth model has an inner log-slope $\alpha = -1.40$ when averaged over 1–2% of the virial radius, consistent with an NFW profile. By contrast, when there are episodic bursts, we find a log-slope $\alpha = -0.63$.

the inner dark matter particles. The fluctuation of the central mass changes the gravitational potential, and if this happens sufficiently quickly (not adiabatically), it boosts the dark matter particles to a higher orbit. The net effect is that this process injects energy into the dark matter particles. We model this process by allowing the tracer particle mass to increase at a constant rate in scale factor, then instantaneously decreasing it. The height of this drop physically corresponds to the gas mass expelled from the central region of the galaxy due to supernova energy. The mass that remains after this sharp decrease corresponds to the stellar mass formed in the burst (which is simply the final stellar mass divided by the number of bursts). After the last burst, the tracer particle's mass remains constant. This is not necessarily physical in the sense that the galaxy's mass can continue to increase, but is motivated by the fact that star formation is less bursty at lower redshifts (Faucher-Giguère 2018). We vary both the number of bursts and the amount of mass expelled in §3.1 to understand the impact of both of these parameters. Rather than making physical assumptions, the range of values we tested for the amount of mass expelled was determined by starting with extremely large values, and decreasing it until core formation ceased.

We assign the burst times by assuming that the time separating bursts is proportional to the dynamical time of the halo. Episodically bursty models with more (fewer) bursts simply assume that the burst timing is a smaller (larger) multiple of the Hubble time. In the model shown in the lower right panel of Figure 1, we assume that the stellar mass forms over five bursts (at $z = 9.9,\ 5.3,\ 2.8,\ 1.3$ and 0.4) and each burst causes $3.6 \times 10^7 M_\odot$ to be expelled from the inner region of the galaxy [1]. The number of bursts that takes place in hydrodynamic simulations which model these processes explicitly can vary based on many factors, but is generally of order 10 bursts. As one example, galaxies in a sample taken from the FIRE simulations underwent $\sim 1-2$ bursts every 200 Myr at $z = 2$ (Sparre et al. 2017). Approximating this as the rate across a galaxy's entire formation history, and assuming that star formation ceases to be bursty at $z \sim 1.3$ (Faucher-Giguère 2018), this yields a typical value of between 20 and 50 bursts.

[1] One can easily see that the minimum mass after burst is gradually increasing with time. In fact, the upper mass immediately before the burst is also increasing with time, but this is not so easily seen with the log-scale of the plot. This makes it seem like the amount of mass being expelled varies with time even though it is constant.

The third and final growth model we employ is the single-burst model. Inspired by stellar age distributions in UFDs (e.g. Sacchi et al. 2021; Brown et al. 2014; Simon 2019; Gallart et al. 2021; Sand et al. 2010; Okamoto et al. 2012; Weisz et al. 2014), these models increase their mass steadily with time (attributed to gas accretion) followed by a single outflow event. The subsequent mass is then held constant until the present day. This model can be considered a limit of the bursty model that is constrained to a single burst.

2.3. *Galaxy Models: Classical and Ultra-faint Dwarf*

We simulate both classical dwarf and ultra-faint dwarf galaxies to study the mechanism of core formation via bursty feedback. The classical dwarf has a $z = 0$ halo mass of $9.2 \times 10^9 M_\odot$. To model a galaxy of this mass with a smooth growth history, we employ the redshift-dependent stellar-to-halo-mass relation (SHMR) described in Moster et al. (2013). To achieve this, we first run a DMO simulation to calculate the halo mass as a function of time. We then use the SHMR to evaluate the corresponding stellar mass and prescribe the growth of the massive particle to match this growth history. The tracer mass enters the simulation at $z = 11$ with a mass of $10^3 M_\odot$ and has a final mass of $3.9 \times 10^6 M_\odot$, as shown in the top right panel of Figure 1 [2]. We place the tracer particle in the simulation no earlier than $z = 11$ because it will be pinned to the potential minimum of the most massive within a manually-defined subvolume. At very early times, the individual halos are closer together and more similar in mass, making it difficult to identify the most massive halo at $z = 0$, which is where we want to place the tracer mass. We do not expect this choice to significantly impact our results because the halo is a small fraction of its $z = 0$ mass. We use a gravitational softening of 0.36 kpc for the massive particle representing the baryon mass of the galaxy, meaning that the majority of the mass is concentrated within 1.1 kpc.

The ultra-faint dwarf (UFD) has a $z = 0$ halo mass of $7.8 \times 10^7 M_\odot$. We adhere to observational constraints on the star formation histories of these systems to determine their stellar mass as a function of time. We prescribe a growth history consistent with the cumulative mass fraction over time of Milky Way (MW) satellites that have a similar present-day halo mass. Specifically, we set the final stellar mass to $1.4 \times 10^3 M_\odot$—

[2] The tracer particle is initialized at the same time of $z = 11$ but at a higher mass (2.3×10^7) for the bursty model shown in the bottom right panel of Figure 1 than the smooth model shown in the top right panel. This is because the first of the five bursts in this model is set to occur at $z = 10$.

consistent with the observed stellar mass of these systems, which ranges from $(0.54 - 7.46) \times 10^3 M_\odot$ (Sales et al. 2017) and within 2σ of both the predictions of semi-analytic models (Ahvazi et al. 2024) and forward modeling of MW satellites (Nadler et al. 2020). In our smooth growth model, the particle mass grows such that 80% of the stellar mass has formed by $z = 7$ and 90% by $z = 5$. To model a single burst for this galaxy, rather than making physical assumptions about when the burst occurs, we manually vary its timing across a wide range of values ($z = 1$ to $z = 8$) to understand how this changes the impact of the outflow on the dark matter density. The amount of mass expelled is initially set at $1.4 \times 10^4 M_\odot$ by making a the details of which are discussed in §3.2, but it is also a parameter that we vary. We also employ a smaller gravitational softening of 0.06 kpc for the massive particle to account for the difference in size between these systems.

2.4. *Characterization of Density Profiles*

We use two independent metrics to characterize the density profiles of the galaxies and assess whether they are cusped or cored. We calculate the inner log-slope, commonly referred to as α (where $\rho \propto r^\alpha$), over 1–2% of the virial radius (Di Cintio et al. 2014; Tollet et al. 2016). This is a reliable metric for cores that are a few percent of the virial radius, but is not sensitive to the presence of smaller cores (given the radius range where α is determined). For this reason, we use a complementary approach of fitting to the core-Einasto model and finding the best-fit core radius r_c (Lazar et al. 2020). This addresses the issue of not detecting smaller cores, but there can still be instances in which the model fit is sufficiently poor that we do not get a reliable estimate of the core radius. Density profiles with slightly irregular shapes will not be well-characterized by a three-parameter model, and in these cases the core radius estimate will also be an imperfect metric. Using both of these measures decreases the bias associated with α or r_c alone.

3. RESULTS

In this section, we present results employing the prescriptive approach described in §2. We split our results into the classical dwarf regime (§3.1) where dark matter cores are often observed (e.g. Walker & Peñarrubia 2011; Amorisco & Evans 2012; Amorisco et al. 2013; Kleyna et al. 2003) and the UFD regime (§3.2) where the dark matter density may or may not be cored, but where star formation is restricted to a small number of bursts (e.g. Brown et al. 2014; Simon 2019; Gallart et al. 2021; Sand et al. 2010; Okamoto et al. 2012; Sacchi et al. 2021; Weisz et al. 2014). Therein, we study how varying the amount of mass expelled per burst, the number of bursts, and the effective size of the galaxy impacts the efficacy of bursty feedback at forming cores.

3.1. *Classical Dwarfs*

Figure 1 provides a visual overview of the smooth (top row) and bursty (bottom row) growth models for the classical dwarf. The top right panel shows the tracer particle's mass as a function of time. In particular the top-right shows the stellar mass inferred from the SMHM relation (black line) (Moster et al. 2013) compared against mass assigned to the tracer particle in the simulation (magenta line). In contrast, the bottom left shows the tracer particle's mass for the episodically bursty model. The left column shows the present-day DM mass projection, produced from a $30 \times 30 \times 30$ kpc box centered on the galaxy. The density at the very center of the halo varies between the top and bottom panels, indicating that the density is strongly cusped. Finally, the second row of the right column shows the corresponding present-day density profile. The grey dashed line marks $2.8\times$ the dark matter particle softening, the point below which numerical effects begin to be important. Looking at the region to the right of the dashed line, we see that the central density profile is strongly cusped for the smooth growth model and cored for the fiducial bursty model—both consistent with expectations.

3.1.1. *Variable Total Mass Outflow Models*

As a first variation on the episodically bursty model, we consider how the number and amplitude of potential variations impact core formation. Specifically, we manually change the strength and frequency of the central potential variations by altering (i) the total number of bursts ranging from 1 to 31 and (ii) the total mass expelled per burst ranging from $0.7 \times 10^7 \mathrm{M}_\odot$ to $7.2 \times 10^7 \mathrm{M}_\odot$. Taken together, this changes the total integrated mass expelled for the tracer particle from $0.7 \times 10^7 \mathrm{M}_\odot$ (for a single burst with the smallest mass expulsion) to $2.2 \times 10^9 \mathrm{M}_\odot$ (for 31 of the most massive bursts). In other words, this tests the impact of changing the total mass ejected from the central region by several orders of magnitude—hence we refer to these scenarios as variable total mass outflow models.

Our results show significant variations in core formation based on our outflow model. For each model, we have calculated both the inner log-slopes and best-fit core radii r_c (Lazar et al. 2020) of the resulting present-day dark matter density profiles. We show the results in terms of both metrics as a function of the amount of

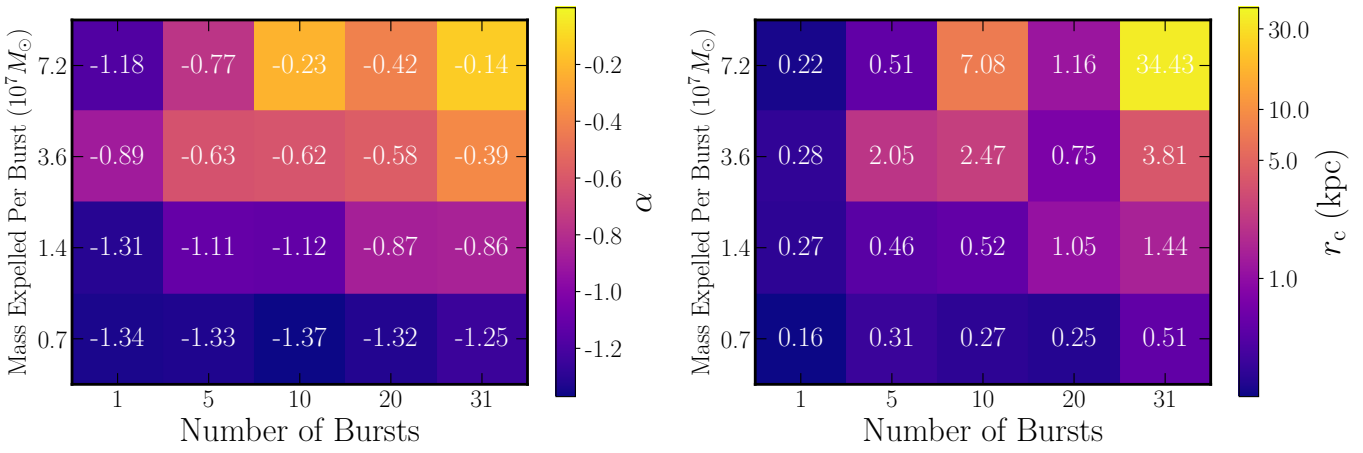

Figure 2. Summary of the inner log-slopes ($\alpha = \frac{d\log\rho}{d\log r}$) best-fit core radii r_c for a classical dwarf galaxy as a function of number of bursts and burst mass.

mass expelled per burst and number of bursts in Figure 2. Several clear trends emerge: galaxies generally have more cored density profiles when they either experience a larger number of bursts (i.e. moving to the right in Figure 2) or more massive bursts (i.e. moving up). As the mass expelled per burst increases, the inner log-slope for the 10, 20, and 31 burst simulations increases from ∼-1.37—1.25 to ∼-0.42—0.14 monotonically. Similarly, the core radius for these simulations increases from ∼0.25–0.51 kpc to ∼1.2–34 kpc. We note that there is also some non-monotonicity, but that this can be mostly attributed to the density profile associated with these models having irregular inner shapes that are not fully described or well-characterized by the three-parameter core-Einasto model. This trend continues to some extent for 1 and 5 bursts. In these regimes, there is still a trend where more massive bursts lead to larger core radii, but the trend is somewhat less pronounced: While the 10, 20, and 31 burst simulations each increase the core radius by a factor of five or more, the single-burst model increases the core radius from ∼0.16–0.28 kpc— less than a factor of two. This result is unsurprising given that increasing the mass-per-burst directly increases the amplitude of the potential fluctuations. For any fixed value of the mass expelled per burst, the largest cores form for the greatest number of bursts. When the mass expelled is held constant at $3.6\times10^6 M_\odot$, for example, the core radius increases from 0.28 to 3.81 kpc as the number of bursts increases from 1 to 31. Similarly, α increases from -0.89 to -0.39.

3.1.2. *Constant Total Mass Outflow Models*

In contrast to the variable total mass outflow models considered in the previous subsection, here we hold the total mass ejected constant while varying the number of bursts and mass-per-burst accordingly. We use the bursty model from Figure 1 as our fiducial run. The total mass expelled is held constant at $1.8\times10^8 M_\odot$ and the number of bursts this takes place over is varied between 1 and 62. In addition, to connect with the previous section, we also present results for the core radius as a function of burst number while holding the mass-per-burst constant using the same total ouflow mass for the $N_{\rm burst} = 5$ model.

Figure 3 shows the trends in core radii as a function of the number of bursts for a variable amount of energy (blue) and a fixed amount of energy (red). The fiducial five-burst model produces a core of 2.1 kpc and has an inner log-slope of -0.63. By contrast, a model expelling the same amount of mass in total over 62 bursts produces a density profile with $\alpha = -1.41$ and best-fit $r_c = 0.19$ kpc. Figure 3 confirms the previously discussed result that larger numbers of bursts generally form larger cores when the mass-per-burst is held fixed (i.e. the blue variable energy line generally increases with burst number) with the non-monotonicity being caused by individual profiles that not very well fit by core-Einasto profiles. However, when the mass-per-burst is reduced with burst number such that the total mass outflow is held constant, a more complex dependence on the number of bursts emerges. Specifically, we find a peak core radius associated with 5 mass outflow events and a decreasing core radius to both larger and smaller number of bursts.

To explore this further, Figure 4 shows the density profiles for the models with constant total mass outflow, ranging from 1 to 5 bursts. The most cored profile is produced when the galaxy undergoes five bursts, shown in red, which has a core radius and inner log-slope of 2.05 kpc and -0.38, respectively. Three bursts produces a profile that is flatter than the strongly cusped smooth-growth model, but is not strongly cored either,

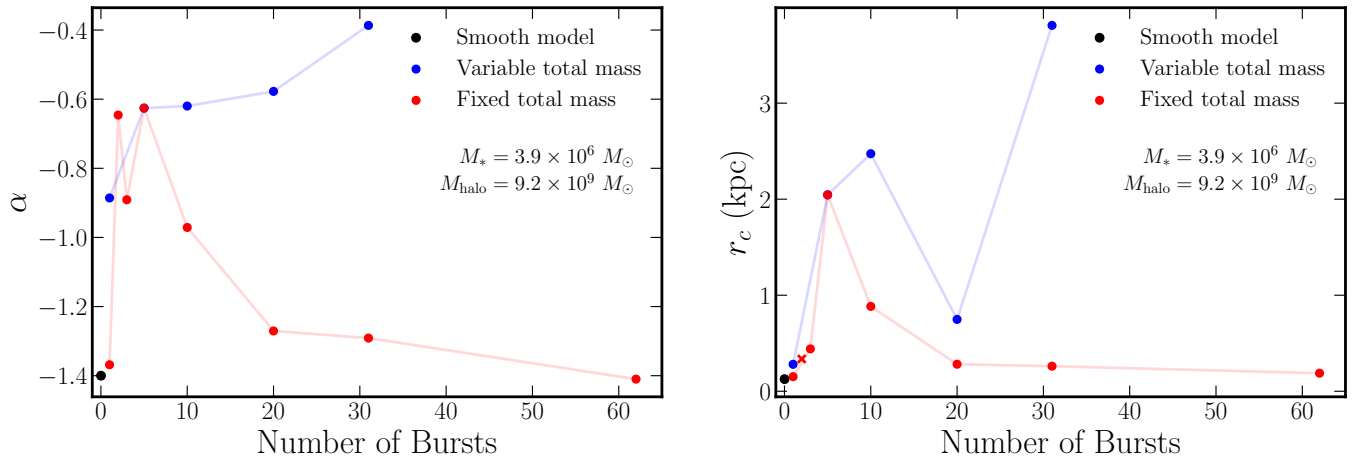

Figure 3. Comparison of the relationship between number of bursts and both the core size (right) and inner log-slope (left) for variable (blue) versus fixed (red) total energy transferred to the dark matter particles via bursty feedback. When the amount of mass expelled in each burst is constant, we find that the profile simply becomes more cored as we increase the number of bursts (increasing the total energy transferred). If instead the mass expelled in each burst is varied such that the total mass expelled is constant, we find a more complex relationship. As the number of bursts is decreased, initially this leads to an increase in the core size. However, if there are fewer than five bursts, this trend reverses. The point marked with an 'x' indicates that for this model, the core-Einasto fit was poor ($Q > 0.08$).

with $\alpha = -0.89$ and $r_c = 0.44$ kpc. The two and one burst models, however, produce profiles that are more cusped. The one burst model producing a profile that has $\alpha = -0.83$ and $r_c = 0.15$ kpc. For the two burst model, the inner log-slope and core radius of $\alpha = -0.65$ and $r_c = 0.37$ kpc are more difficult to interpret due to the shape of the density profile. From Figure 4, we can see that the density profile plateaus from 0.5 to 2 kpc, which overlaps with the range where the slope is calculated, but it begins to rise again for smaller radii. This means the calculated value of α does not characterize this density profile well, which is why we present the results in terms of the core radius as well.

The trend where increasing the number of bursts makes a more cored profile reverses after 5 bursts. The reversal after 5 bursts is perhaps unsurprising. Indeed, in our constant total mass outflow models, the limit of $N_{\rm bursts} \to \infty$ becomes indistinguishable from a smooth growth model—which we have already demonstrated to form a cusp. What is more surprising is that core formation is mitigated in the limit where the number of bursts approaches only a single event (or very small number of events). We discuss and explore this further in the discussion section.

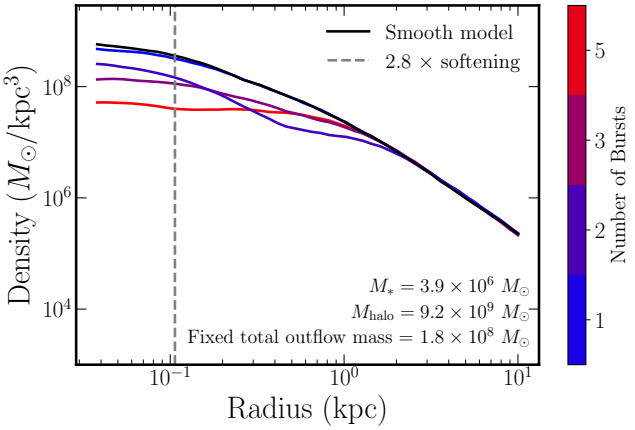

Figure 4. Present-day density profiles for a fixed amount of total mass expelled ($1.8 \times 10^8 M_\odot$) over time and a varied number of bursts. As the number of bursts decreases (and therefore, the amount of mass expelled per burst increases) larger cores form. However, cores stop forming altogether when the number of bursts becomes very small (i.e. ∼1–2) despite the large amount of mass being expelled. The gray dashed line indicates the radius at which numerical softening effects begin to impact the results.

3.2. *Ultra-Faint Dwarfs*

Using our findings from the classical dwarf regime as a guide, we vary the time and size of a single burst in an ultra-faint dwarf galaxy to determine in what part of that parameter space core formation is possible, and how that compares to what is known about these systems. In all simulations described below, the galaxy has a final halo mass of $7.8 \times 10^7 M_\odot$ and to match observational mass measurements of the MW satellites that motivated this analysis, we prescribe a final stellar mass of $1.4 \times 10^3 M_\odot$. We assume that all of the ultrafaints have 95% gas fractions—giving them total pre-burst masses of 1.54×10^4, an outflow mass of $1.4 \times 10^4 M_\odot$, and a post-burst mass of $1.4 \times 10^3 M_\odot$. We test three single-

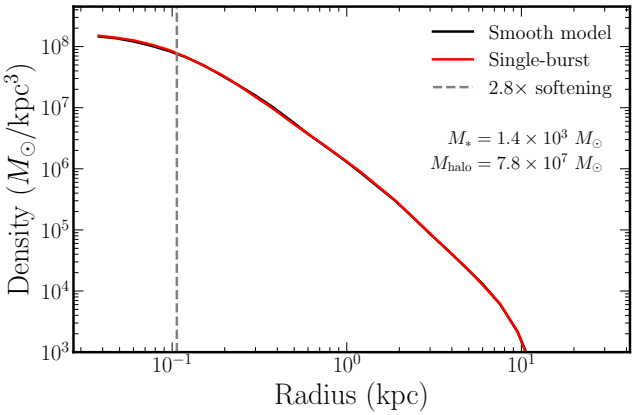

Figure 5. Comparison of the present-day dark matter density profile for an ultrafaint dwarf galaxy if it has a smooth growth history (black) or forms in a single burst at $z = 7$ (red) resulting in the ejection of $1.4 \times 10^4 M_\odot$. The density profiles are both cusped with $r_c = 0.07, 0.05$ and $\alpha = -1.25, -1.35$ for the smooth-growth and single-burst models, respectively.

burst models where the outflow from the galaxy occurs at $z = 8$, 7 and 6. We compare the present-day density profiles of these models with that of a smooth model that also adheres to observational constraints on the formation histories of these systems. The mass is increased at each timestep such that 80% of the stellar mass forms by $z = 7$, and 90% forms by $z = 3$. We find that none of the three single-burst models form a core, with α between -1.35 and -1.15 and r_c between 0.05 and 0.08 kpc.

Finally, we run a suite of simulations to determine at what point, in terms of mass expelled and timing of the burst, cores begin to form. The results, in terms of the inner log-slope and core radius, are summarized in Figure 6 as a function of the time at which the burst occurs. An approximate upper bound on how late a single burst could have occurred based on observed stellar ages of these systems is marked with a black vertical line ($z = 6$). The horizontal line at $\alpha = -0.8$ marks where the density profiles would begin to be considered cored. It is important to note, however, that there is no precise value that is a perfect threshold. The smallest amount of mass expelled that forms a core is $1.2 \times 10^6 M_\odot$, which produces a density profile with $\alpha = -0.68$ if the burst occurs at $z = 3$. The same mass expelled at $z = 5$ nearly produces a cored profile, with $\alpha = -0.86$. We find that the earliest burst to form a core is one at $z = 5$, with $2.9 \times 10^7 M_\odot$ and $\alpha = -0.12$. The shaded region in Figure 6 represents the intersection of α consistent with a cored profile and burst times consistent with observational constraints on these systems. The region is empty as none of the models we ran in this analysis generated cores with an early, single burst.

4. DISCUSSION

From Figure 5, we can see that a single, or very small number, of bursty outflows does not produce a core that persists today if we make reasonable assumptions about how and when this occurs for an ultra-faint dwarf analogous to one of the Local Group satellites. In addition to the amount of mass that can be expelled, we also have observational constraints on when this can happen from the cumulative star formation histories (e.g., Sacchi et al. 2021). All of these systems formed the majority of their stellar mass by the midpoint of reionization ($z = 7.7$) with many of them having formed more than 80% their stellar mass by this point. Therefore, $z = 7$ is perhaps even a late limit for what could be considered a reasonable time for a single burst of star formation to take place in one of these systems. Despite these assumptions, we find that the density profile remains strongly cusped. This is an important finding, given that similar Local Group satellites have recently been found to have cored density profiles (Almeida et al. 2024). While we have observational constraints that lead us to the assumptions above, we also can exploit the flexibility of our method to gain further insights as to why these systems fail to form cores by asking: when can one burst form a core? First, we will discuss the results from varying the size and timing of this burst in the ultra-faint regime, then we will discuss how these results compare to our findings in the classical dwarf regime.

Figure 6 shows that as we simultaneously vary the mass expelled in the burst and the time at which this occurs, there is some part of the parameter space for which this burst forms a core. However, as shown by the shaded grey region, there is no overlap between bursts that take place at a reasonable time and bursts that form a core. Notably, this result holds regardless of the total amount of mass expelled, even in the case of expelling $2.9 \times 10^7 M_\odot$, which is $> 10\%$ of the halo mass, and $\sim 10^4\times$ the assumed $z = 0$ stellar mass. Even in this case, a burst at $z = 5$ forms a core while a burst at $z = 6$ does not. This result implies that our initial assumptions about the amount of mass that can be expelled carry less importance because the timing of the burst acts as a secondary barrier to core formation in these systems. The amount of mass expelled, to some extent, dictates whether or not core formation is possible. We see this from the dark purple points in Figure 6 all lying below the dotted line, even as the time of the burst varies. However, the lack of core formation seen prior to $z = 6$

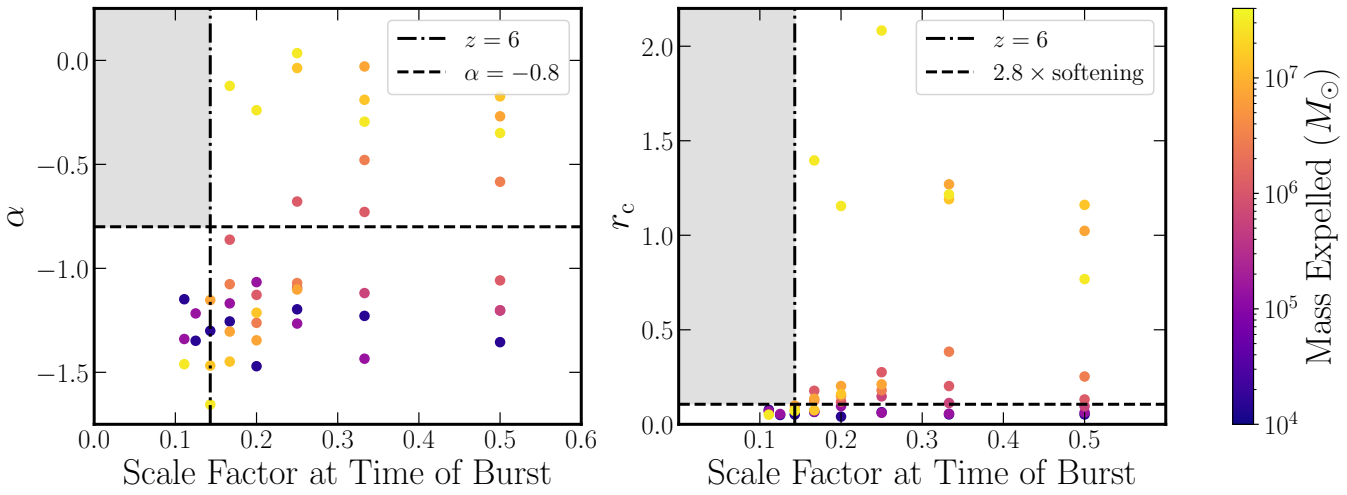

Figure 6. *Left:* Inner dark matter density profile slope, α, as a function of scale factor at which the outflow occurs. Notably, the upper left region is unoccupied, indicating the dark matter cores do not easily form when bursty activity is relegated to the earliest times even when extreme mass outflow events are considered. *Right:* Best-fit values for the core radius r_c as a function of scale factor at the time at which the outflow occurs. Similarly, cores of appreciable size do not form when the bursts are restricted to occur at early times regardless of the size of the outflow.

indicates this is not all that matters, and this secondary barrier that we find shows that bursty feedback's ability to resolve the tension in this limit is not only dependent on the stellar mass (as this has typically been viewed). We also note that while there is no universally accepted cutoff value for calling a profile cored, typical values in the literature are between $\alpha \gtrsim -1.0$ and -0.8, and our conclusions above are independent of this choice.

Given that we established in Section 3.1 that this method of modeling the impact that bursty star formation has on the central potential can turn dark matter cusps into cores (Figure 1), we wish to understand why it is so difficult to form cores in the limiting case of systems like the Local Group ultra faints. To do this, we can use the insights we gained from the classical dwarf regime. Recall that we studied galaxies of this mass for two reasons:

- Previous studies using hydrodynamic simulations (e.g., NIHAO, FIRE-2) have shown that bursty feedback can modify the density profiles beginning at the classical dwarf mass scale, which makes this halo an excellent candidate to validate our methodology and show that cores can form with this approach in the regime where we expect this to be possible.

- Once we show our fiducial bursty model produces a cored density profile in the classical dwarf regime, we can take advantage of the flexibility of our method to smoothly vary important parameters such as the amount of mass expelled and the number of bursts to gain a deeper understanding of where in this space cores do and do not form.

The second point is what allows us to better understand the inability of one, or a small number, of bursty outflows to form a core in the ultra-faint regime while adhering to observational constraints. Analytic modeling of single outflows has largely focused on the energetics of such an episode (the amount of gas in the disk and the supernova energy available to drive an outflow). The power of our approach is that it allows us to directly answer the question of interest: If the total energy injected by the outflow to the DM particles is held fixed, does the number of bursty outflows still matter? It can be seen from Figure 4 that initially, when decreasing the bursts from 62 to 5, the dominant effect in terms of the strength of core formation is the amount of mass being expelled: fewer, larger bursts are more impactful. Critically, we find that this trend reverses as the number of bursts is decreased further. For fewer than five bursts, the dominant factor in determining how many of the inner-region DM particles that can be impacted is the number of bursts, not the size of them.

We note that there are some limitations associated with modeling the impact of bursty feedback on the DM particles in this manner: While we make physical arguments for the timing and magnitude of the bursts in our models, they may not be identical to those that would occur in an observed system. We prescribe a set of times for which the central potential is changed dramatically and suddenly, however, nothing physically causes this burst to occur. In particular, we do not impose any

constraints on the times at which bursts can happen. As described in Section 2.2, the list of burst times was created by assuming that a burst happens with temporal spacings proportional to the halo dynamical time. One potential consequence of this is that the models with a larger number of bursts in particular have bursts occurring later than may be physically realistic.

The generalizability of our results is limited in two ways. Firstly, we do not vary the formation history (in other words, the set of initial conditions) for either halo. We would not expect this to dramatically affect our qualitative conclusions. Secondly, our simulations are of field galaxies, not satellites like the UFDs in the Local Group which in part motivated the analysis. The role of the environment and the impact that this may have on our results is yet to be tested.

Using our novel approach, we find that galaxies undergoing multiple episodes of bursty outflows can have cored density profiles while equivalent models that undergo just one or a smaller number of outflows do not form cores with the same efficacy. Most importantly, we find that in galaxies of comparable mass to the ultra-faint satellite galaxies within our Local Group, bursty feedback does not appear to alleviate the tension while adhering to the observational constraints regarding how and when these systems formed.

5. CONCLUSIONS

In this paper, we introduce a novel approach to modeling the impact of bursty outflows on the orbits of DM particles in the inner region of dwarf galaxies to identify the regimes in which bursty feedback can and cannot turn cusps into cores. We model the gravitational impact of baryons with a massive tracer particle, which allows us to maintain control over how and when these bursty outflows occur within a cosmological environment. This technique sits at the intersection of the two avenues bursty feedback has typically been studied through: cosmological simulations where baryonic processes are modeled explicitly and the more controlled analytic or idealized modeling of the impact a changing gravitational potential has on the DM particle orbits. Specifically, we introduce this method to evaluate the ability of a single burst to form cores under realistic conditions for an ultra-faint dwarf galaxy with a key constraint: the stars form in a short period of time and in the early universe. We introduce two suites of modified DMO simulations: a classical dwarf and ultra-faint dwarf analog, and study how varying the prescribed evolution of the tracer particle (representing the baryon mass) in a way that corresponds to different star formation histories impacts the present-day dark matter density profile. Our key findings are as follows:

- Our simplified model reproduces the cusp-to-core transformation for a galaxy of halo mass $\approx 10^{10} M_{\odot}$, which is the regime where we expect this to take place based on the results of hydrodynamic simulations that model baryonic physics (including bursty feedback) explicitly. We find our smooth-growth model produces a cusp, while our fiducial bursty model produces a core.

- Whether or not a core forms depends on the amount of mass expelled in the burst and how many bursty outflows there are. All else equal, a larger number of bursts or a larger amount of mass expelled produces a more cored profile at present-day. This result was consistent across both metrics that we used to quantify the strength of core formation: the inner log-slope (α) and the best-fit value for the core radius ($r_{\rm c}$).

- A single burst (or small number of bursts) did not form a core for the $10^{10} M_{\odot}$ halo. One burst of varying mass expelled between 0.72–7.2 $\times 10^{7} M_{\odot}$ did not form a core, while the fiducial five-burst model did.

- Holding the total mass expelled over all the bursts fixed (and therefore holding the total energy transferred irreversibly to the DM particles fixed), we still find a dependence on the number of bursts that the mass is expelled over. We find that for five or more bursts, it is more effective to have fewer, larger bursts. However, for fewer than five bursts, the profiles become cusped once again despite the large amount of mass being expelled.

- Applying this method to an ultra-faint galaxy analogous to the satellites within our Local Group, we find that a single burst is insufficient to transform the DM density profile if we make realistic assumptions about how and when the burst occurs.

- By varying the parameters of our single burst models to understand why we did not see core formation, we discover two barriers for an ultra-faint dwarf with a tightly constrained SFH like the satellites of our Local Group. The initial barrier is the amount of mass that must be expelled to significantly impact the DM density. We find that core formation took place only for model in which the burst expelled a mass of 1.2 $\times 10^{6} M_{\odot}$ or more. In addition to this, there is a second

barrier, which is that the burst must happen sufficiently late. Disregarding any constraints on the size of the burst based on energetics, we find that cores did not form for any of our models in which the burst occurred prior to $z = 5$. Given that the SFHs of the Local Group satellites are largely constrained to before reionization, this result indicates that a single burst of star formation is insufficient to explain the cored density profiles of these systems.

By employing our modified DMO approach to the limit of extremely low-mass systems with SFHs strongly constrained to early times, we have shown that bursty feedback is insufficient to transform dark matter cusps to cores, and therefore, is insufficient to alleviate the tension between ΛCDM predictions and observations.

REFERENCES

Ahvazi, N., Benson, A., Sales, L. V., et al. 2024, MNRAS, 529, 3387, doi: 10.1093/mnras/stae761

Almeida, J. S., Trujillo, I., & Plastino, A. R. 2024, Astrophys. J. Lett., 973, L15, doi: 10.3847/2041-8213/ad66bc

Amorisco, N. C., Agnello, A., & Evans, N. W. 2013, MNRAS, 429, L89, doi: 10.1093/mnrasl/sls031

Amorisco, N. C., & Evans, N. W. 2012, MNRAS, 419, 184, doi: 10.1111/j.1365-2966.2011.19684.x

Azartash-Namin, B., Engelhardt, A., Munshi, F., et al. 2024, ApJ, 970, 40, doi: 10.3847/1538-4357/ad49a5

Brown, T. M., Tumlinson, J., Geha, M., et al. 2014, ApJ, 796, 91, doi: 10.1088/0004-637X/796/2/91

Bullock, J. S., & Boylan-Kolchin, M. 2017, ARA&A, 55, 343, doi: 10.1146/annurev-astro-091916-055313

Burger, J. D., Zavala, J., Sales, L. V., et al. 2022, MNRAS, 513, 3458, doi: 10.1093/mnras/stac994

Chan, T. K., Kereš, D., Oñorbe, J., et al. 2015, MNRAS, 454, 2981, doi: 10.1093/mnras/stv2165

Di Cintio, A., Brook, C. B., Macciò, A. V., et al. 2014, MNRAS, 437, 415, doi: 10.1093/mnras/stt1891

Faucher-Giguère, C.-A. 2018, MNRAS, 473, 3717, doi: 10.1093/mnras/stx2595

Fitts, A., Boylan-Kolchin, M., Elbert, O. D., et al. 2017, MNRAS, 471, 3547, doi: 10.1093/mnras/stx1757

Gallart, C., Monelli, M., Ruiz-Lara, T., et al. 2021, ApJ, 909, 192, doi: 10.3847/1538-4357/abddbe

Governato, F., Brook, C., Mayer, L., et al. 2010, Nature, 463, 203, doi: 10.1038/nature08640

Governato, F., Zolotov, A., Pontzen, A., et al. 2012, MNRAS, 422, 1231, doi: 10.1111/j.1365-2966.2012.20696.x

Hahn, O., & Abel, T. 2011, MNRAS, 415, 2101, doi: 10.1111/j.1365-2966.2011.18820.x

Hayward, C. C., & Hopkins, P. F. 2017, MNRAS, 465, 1682, doi: 10.1093/mnras/stw2888

Hopkins, P. F., Kereš, D., Oñorbe, J., et al. 2014, MNRAS, 445, 581, doi: 10.1093/mnras/stu1738

Jahn, E. D., Sales, L. V., Marinacci, F., et al. 2023, MNRAS, 520, 461, doi: 10.1093/mnras/stad109

Kleyna, J. T., Wilkinson, M. I., Gilmore, G., & Evans, N. W. 2003, ApJL, 588, L21, doi: 10.1086/375522

Lazar, A., Bullock, J. S., Boylan-Kolchin, M., et al. 2020, MNRAS, 497, 2393, doi: 10.1093/mnras/staa2101

Moore, B. 1994, Nature, 370, 629, doi: 10.1038/370629a0

Moster, B. P., Naab, T., & White, S. D. M. 2013, MNRAS, 428, 3121, doi: 10.1093/mnras/sts261

Nadler, E. O., Wechsler, R. H., Bechtol, K., et al. 2020, ApJ, 893, 48, doi: 10.3847/1538-4357/ab846a

Navarro, J. F., Eke, V. R., & Frenk, C. S. 1996a, MNRAS, 283, L72, doi: 10.1093/mnras/283.3.L72

Navarro, J. F., Frenk, C. S., & White, S. D. M. 1996b, ApJ, 462, 563, doi: 10.1086/177173

Oñorbe, J., Boylan-Kolchin, M., Bullock, J. S., et al. 2015, MNRAS, 454, 2092, doi: 10.1093/mnras/stv2072

Okamoto, S., Arimoto, N., Yamada, Y., & Onodera, M. 2012, ApJ, 744, 96, doi: 10.1088/0004-637X/744/2/96

Planck Collaboration, Aghanim, N., Arnaud, M., et al. 2016, A&A, 594, A11, doi: 10.1051/0004-6361/201526926

Pontzen, A., & Governato, F. 2012, MNRAS, 421, 3464, doi: 10.1111/j.1365-2966.2012.20571.x

—. 2014, Nature, 506, 171, doi: 10.1038/nature12953

Read, J. I., & Gilmore, G. 2005, MNRAS, 356, 107, doi: 10.1111/j.1365-2966.2004.08424.x

Reid, B. A., Percival, W. J., Eisenstein, D. J., et al. 2010, MNRAS, 404, 60, doi: 10.1111/j.1365-2966.2010.16276.x

Rose, J. C., Torrey, P., Vogelsberger, M., & O'Neil, S. 2023, MNRAS, 519, 5623, doi: 10.1093/mnras/stac3634

Sacchi, E., Richstein, H., Kallivayalil, N., et al. 2021, ApJL, 920, L19, doi: 10.3847/2041-8213/ac2aa3

Sales, L. V., Navarro, J. F., Kallivayalil, N., & Frenk, C. S. 2017, MNRAS, 465, 1879, doi: 10.1093/mnras/stw2816

Sales, L. V., Wetzel, A., & Fattahi, A. 2022, Nature Astronomy, 6, 897, doi: 10.1038/s41550-022-01689-w

Sand, D. J., Seth, A., Olszewski, E. W., et al. 2010, ApJ, 718, 530, doi: 10.1088/0004-637X/718/1/530

Shen, X., Hopkins, P. F., Necib, L., et al. 2024, ApJ, 966, 131, doi: 10.3847/1538-4357/ad2fb1

Simon, J. D. 2019, ARA&A, 57, 375, doi: 10.1146/annurev-astro-091918-104453

Somerville, R. S., & Davé, R. 2015, ARA&A, 53, 51, doi: 10.1146/annurev-astro-082812-140951

Sparre, M., Hayward, C. C., Feldmann, R., et al. 2017, MNRAS, 466, 88, doi: 10.1093/mnras/stw3011

Spergel, D. N., & Steinhardt, P. J. 2000, PhRvL, 84, 3760, doi: 10.1103/PhysRevLett.84.3760

Springel, V. 2010, MNRAS, 401, 791, doi: 10.1111/j.1365-2966.2009.15715.x

Springel, V., White, S. D. M., Jenkins, A., et al. 2005, Nature, 435, 629, doi: 10.1038/nature03597

Tollet, E., Macciò, A. V., Dutton, A. A., et al. 2016, MNRAS, 456, 3542, doi: 10.1093/mnras/stv2856

Tulin, S., & Yu, H.-B. 2018, PhR, 730, 1, doi: 10.1016/j.physrep.2017.11.004

Vogelsberger, M., Marinacci, F., Torrey, P., & Puchwein, E. 2020, Nature Reviews Physics, 2, 42, doi: 10.1038/s42254-019-0127-2

Vogelsberger, M., Zavala, J., Simpson, C., & Jenkins, A. 2014, MNRAS, 444, 3684, doi: 10.1093/mnras/stu1713

Walker, M. G., & Peñarrubia, J. 2011, ApJ, 742, 20, doi: 10.1088/0004-637X/742/1/20

Weinberger, R., Springel, V., & Pakmor, R. 2020, ApJS, 248, 32, doi: 10.3847/1538-4365/ab908c

Weisz, D. R., Dolphin, A. E., Skillman, E. D., et al. 2014, ApJ, 789, 147, doi: 10.1088/0004-637X/789/2/147